Analyst

ROYAL SOCIETY OF CHEMISTRY

PAPER

View Article Online
View Journal | View Issue

Cite this: *Analyst*, 2023, **148**, 5496

Rapid fabrication of hydrophobic/hydrophilic patterns on paper substrates for paper spray mass spectrometry†

Austin Arias,‡ Peyton E. Windham,‡ Natalie A. Cheyne and William M. Gilliland, Jr. *

A simple, rapid chemical coating and patterning method was developed and optimized for paper-based substrates for use in paper spray mass spectrometry (PS-MS). A variety of chlorosilanes were explored for coating paper substrates, and their effectiveness in forming hydrophobic surfaces was characterized *via* contact angle goniometry, scanning electron microscopy, and energy dispersive X-ray spectroscopy. Trichloromethylsilane was selected as the primary coating agent because of the short time required to produce a hydrophobic surface (contact angle > 130°), as well as the ease of patterning. Patterning was performed using 3D-printed masks and an oxygen/plasma cleaner. Optimal mask thickness and oxygen/plasma cleaning parameters were determined to produce channels varying from 0.5 to 2.5 mm in width. The effectiveness of the patterned substrates for PS-MS was determined *via* analysis of four antiretrovirals: emtricitabine, lamivudine, efavirenz, and dolutegravir. Calibration curves were made for each antiretroviral at varying channel widths, and the limits of detection and limits of quantification for each drug were determined. These results show that this patterning method results in an average 7.2-fold improvement in sensitivity and an average 190-fold improvement in limits of detection over uncoated paper substrates in a neat matrix. In a proof-of-concept experiment, calibration curves were generated for each antiretroviral in urine. A patterned paper substrate with a 2-mm channel resulted in an average 7.4-fold improvement in sensitivity and an average 18-fold improvement in limits of detection over uncoated paper substrates.

Received 27th June 2023,
Accepted 14th September 2023

DOI: 10.1039/d3an01071f

rsc.li/analyst

Introduction

Ambient ionization mass spectrometry (MS) has emerged over the past two decades as a powerful method for rapid detection of an analyte with minimal sample preparation.[1,2] The development of ambient ionization MS began with desorption electrospray ionization (DESI)[3,4] and direct analysis in real time (DART)[5] and has since expanded to include a large number of other techniques. Since its development in 2010, paper spray (PS) has become one of the most widely used ambient ionization techniques.[6] In a typical PS experiment, a sample is spotted on a triangular paper substrate and allowed to dry, which is followed by the addition of a solvent and application of high voltage, resulting in a spray from a corner of the paper that can be detected by a mass spectrometer. In addition to rapid detection and simple operation, PS has the added advantage of inexpensive operation, using only paper substrates, high voltage, and small volumes of solvents. The benefits of PS-MS have led to its development for a range of applications including forensics,[7–11] environmental monitoring,[12–15] drug screening and clinical diagnostics,[16–22] as well as reaction monitoring.[23–27]

An attractive feature of PS is the ability to enhance analysis by chemical or physical modification of the paper substrate. One approach to paper modification is to imbue the paper with particles, often using starch as an adhesive agent. Several groups have used this strategy to coat paper substrates with polystyrene microspheres,[28,29] zirconia,[30] silica,[31,32] nanoparticles,[33,34] and metal organic frameworks.[35,36] Another common strategy for paper modification has been to take advantage of the reactivity of surface hydroxyl groups and chemically functionalize the surface. The goal of chemical coating has often been to produce a hydrophobic surface,[11,37–39] though several groups have also modified substrates with the goal of increasing specificity for a range of targets including biomolecules and other polar compounds.[40–42]

One modification to paper substrates for PS-MS that has improved analytical performance is the introduction of hydrophilic channels surrounded by hydrophobic barriers to direct

Department of Chemistry, Furman University, Greenville, SC 29613, USA.
E-mail: mac.gilliland@furman.edu

†Electronic supplementary information (ESI) available. See DOI: https://doi.org/10.1039/d3an01071f

‡These authors contributed equally to this work.

the solvent toward the inlet. Without directing solvent flow, the solvent will spread throughout the entirety of the substrate. Multiple groups have addressed this issue by creating hydrophobic barriers from photoresist,[43] paraffin,[44] wax,[45] and combinations of the latter two.[46] Photoresists have been shown to increase background in the mass spectrometry signal, limiting sensitivity *via* ion suppression, and paraffin and wax must be heated to fully penetrate the paper, which may reduce dimensional control. In addition, Jackson, *et al.* noted in a recent paper that the wax printer used for much of this work is now discontinued.[47] With the exception of photoresist, there is a notable lack of published approaches to chemically pattern paper substrates for PS-MS. A number of chemical patterning approaches have been developed for other microfluidic paper-based analytical devices (μPADs),[48–50] but very few of these have been applied to PS-MS.

Herein, a simple approach is introduced to chemically coat and pattern paper substrates for PS-MS. Paper substrates are first chemically modified to become hydrophobic *via* reaction with trichloromethylsilane (TCMS). Following coating, hydrophilic channels are created in the substrates by controlled oxidation of the coating *via* 3D-printed masks and treatment by oxygen/plasma. Channel geometry is varied to test sensitivity and limits of detection for a set of antiretrovirals (ARVs) used to treat HIV in both methanol/water and urine.

Experimental

Chemicals and materials

Methanol (LC-MS), water (LC-MS), formic acid (LC-MS), and hexane (reagent grade) were obtained from Fisher Scientific (Pittsburgh, PA, USA). Whatman 1 filter paper (110 mm diameter) and Petri dishes (100 mm diameter) were also obtained from Fisher Scientific. Trichloromethylsilane (TCMS), trichlorophenylsilane (TCPhS), trichlorooctylsilane (TCOS), and trichloro-(3,3,3-trifluoropropyl)-silane (TCFS) were obtained from Sigma Aldrich (St. Louis, MO, USA). L-Dopa, efavirenz (EFV), dolutegravir (DTG), emtricitabine (FTC), and lamivudine (3TC) were also obtained from Sigma. The ARVs have the following C_{max} values from FDA drug label data: 4.1 μg mL^{-1} (EFV), 3.7 μg mL^{-1} (DTG), 1.8 μg mL^{-1} (FTC), 1.4 μg mL^{-1} (3TC).[51] Pooled human urine was obtained from Innovative Research (Novi, MI, USA). Plastic masks were designed in Solidworks 2020 (Solidworks Corporation, Waltham, MA, USA) and sliced for 3D printing using PrusaSlicer (Prusa Research, Czech Republic). Prusament polylactic acid (PLA) was used for all masks on a Prusa MK3S printer. Food coloring obtained from a local grocery store was added to water to create a colored solution to view the channels on the paper substrates.

Coating and patterning

Filter paper substrates were cut into quarters prior to coating and placed in a Petri dish, with one to three quarter papers per dish. A volume of 15 mL of 5, 10, or 50 mM of each silane in hexane was added to the Petri dish with immersion times ranging from 5 to 120 minutes. The papers were removed with tweezers and were hung to dry in a hood.

Coated papers were characterized *via* contact angle goniometry (CAG), scanning electron microscopy (SEM), and energy-dispersive X-ray spectroscopy (EDS). CAG was performed with a KSV Theta Optical Tensiometer. Contact angles were measured for 5 μL drops of deionized water using Attension Theta software. A minimum of three replicates were collected for each sample. SEM images and EDS spectra were acquired with a JEOL JSM-IT-200LA equipped with a JEOL JED-2300 Dry SDD EDS detector.

For patterning optimization, papers were cut into rectangles (45 × 30 mm). For paper spray substrates, the papers were cut into isosceles triangles (8 mm base × 16 mm height). The paper substrates were then placed in 3D-printed PLA cartridges used as masks. The masks had nominal channel widths of 0.5, 1.0, 1.5, 2.0, and 2.5 mm. The paper in the cartridge was then exposed to oxygen/plasma using a plasma cleaner (PDC-32G, Harrick Plasma, Ithaca, NY) for 5 to 20 s set at low, medium, or high intensity. The chamber was evacuated to <0.2 Torr *via* a roughing pump (IDP-3 dry scroll pump, Agilent Technologies, Santa Clara, CA, USA). Oxygen gas (~200 Torr) was then added to the chamber *via* a needle valve. The valve to the oxygen was closed, and the chamber was evacuated to <0.2 Torr. Oxygen (~1 Torr) was then added to the chamber. The valve was closed once more, and the chamber was evacuated to <0.2 Torr. The RF voltage was then turned on and set at the desired intensity. The valve to the oxygen was reopened, creating a plasma in the chamber at a pressure of ~1 Torr. After the desired exposure time, the voltage was turned off, and the chamber was vented to remove the samples. The papers were removed from the cartridges and stored in Petri dishes under ambient conditions until further analysis.

Paper spray mass spectrometry

For our initial tests, standard calibration solutions were prepared in 50/50 methanol/water (v/v) at the following concentrations: 0 (blank), 10, 25, 50, 100, 250, 500, and 1250 ng mL^{-1}. Each solution contained FTC, 3TC, EFV, and DTG plus L-Dopa as an internal standard at a concentration of 250 ng mL^{-1}. A volume of 6 μL of each standard was spotted onto the center of the paper substrates and allowed to dry before analysis. For urine samples, standard calibration solutions with the four ARVs were prepared in urine at the following concentrations: 0 (blank), 100, 250, 500, 1250, 2500, and 5000 ng mL^{-1}, with each having L-Dopa as an internal standard at 500 ng mL^{-1}. A volume of 6 μL of urine was spotted onto the center of paper substrates and allowed to dry prior to analysis.

All paper spray mass spectrometry experiments were performed with an LTQ Velos Pro Dual Ion Trap Mass Spectrometer (Thermo Fisher Scientific, Waltham, MA). A voltage of +4 kV was applied for all experiments *via* a copper clip, held in place by a laboratory clamp. The spray solvent for all analyses was 50/50 methanol/water (v/v) spiked with 0.1% formic acid and was placed manually on the paper *via* micropipette. Prior to pipetting, the solvent was kept on ice during

the analysis. Uncoated paper substrates required 20 μL of solvent to sustain an electrospray for the period of analysis. The volume applied to patterned substrates depended on channel width, ranging from 5 μL for the 0.5 mm wide channels to 8 μL for the 2.5 mm wide channels. MS/MS transitions for each target analyte were as follows: *m/z* 420 → *m/z* 277 (DTG), *m/z* 316 → *m/z* 244 (EFV), *m/z* 248 → *m/z* 130 (FTC), *m/z* 230 → *m/z* 112 (3TC), and *m/z* 198 → *m/z* 181 (L-Dopa). L-Dopa was chosen as a cost-effective internal standard. Data were acquired *via* a method in which the electrospray voltage was off for 0.1 min, turned on for 1.0 min, and then turned off for 0.1 min, creating a peak that could be integrated. The areas of the peaks for the analytes and internal standard were integrated using Freestyle Software (Thermo Fisher Scientific).

Results and discussion

Hydrophobic coating

The initial approach for creating patterned paper was to first coat an entire paper with hydrophobic reagents, followed by controlled removal of a portion of the coating using a mask during oxygen/plasma exposure. The reaction of chlorosilanes with surface hydroxyl groups is well-established and robust, so we explored four chlorosilane reagents for surface modification: TCMS, TCOS, TCPhS, and TCFS. After each reaction, the hydrophobicities of the papers were measured *via* CAG. We tested a range of reagent concentrations and coating times, shown in Fig. 1. Each data point represents an average of three contact angle measurements. Missing data points indicate that a contact angle was not measurable (*i.e.*, the paper remained hydrophilic). Error bars were removed for graph readability. Papers modified with TCOS and TCMS showed consistently larger maximum contact angles than the other two silanes (≳130°), indicating a more hydrophobic surface. In addition, these two silanes produce a hydrophobic surface after just 5 minutes of coating. TCFS-modified papers showed consistent contact angles of ~120°, with a higher concentration necessary to produce that contact angle at shorter times. TCPhS-modified paper substrates were overall the least hydrophobic and required 30 minutes for the contact angle to reach a maximum at the highest concentration (50 mM). Sample contact angle images for silane-modified paper are shown in Fig. 2.

The morphology of the paper surfaces was characterized by scanning electron microscopy, and sample images for each type of modified paper are shown in Fig. 3. The fibers of each of the coated papers are visible in the images, and the morphology of the coated papers is similar to that of the uncoated paper. Thus, the morphology observed by SEM suggests that the hydrophobicity of the paper is due to a thin layer of silanes. In the case of the TCMS-coated paper, there were small clumps of material visible on the surface that are not present on any of the other paper substrates, likely aggregates formed from polymerization of TCMS, creating a rougher surface than the other silanes. TCMS contains the simplest chain of the four silane reagents (a methyl group), so it was

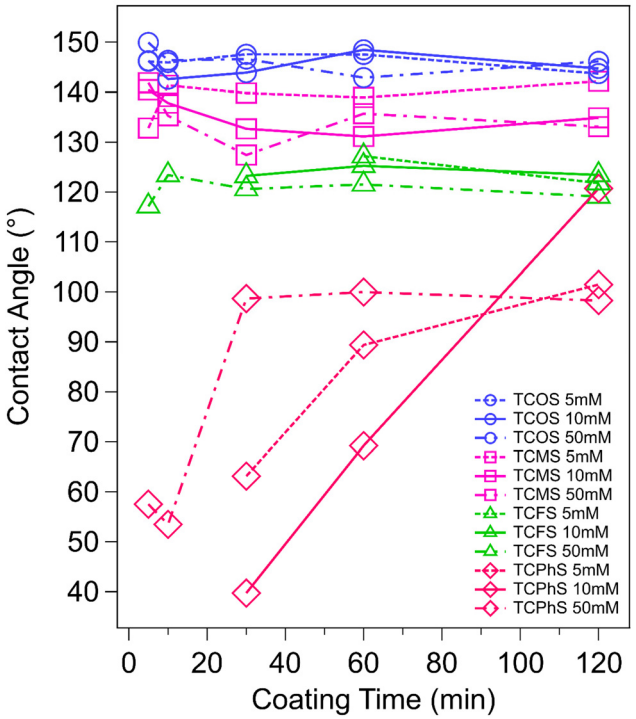

Fig. 1 Contact angle as a function of coating time and silane concentration for paper substrates coated with four silanes: trichloromethyl silane (TCMS), trichlorophenylsilane (TCPhS), trichlorooctylsilane (TCOS), and trichloro-(3,3,3-trifluoropropyl)-silane (TCFS).

expected that TCMS might produce the least hydrophobic surface. Previous research has shown that both surface chemistry and roughness play a role in hydrophobicity.[52] Thus, the observed images suggest that the hydrophobicity of the TCMS-coated papers may be a combination of the modification of the surface and an increase in surface roughness. Given the small size of the methyl group relative to the other silane side chains (phenyl, trifluoropropyl, and octyl), there may be a denser coating of TCMS at the surface due to reduced steric interaction of the side chains. Thus, increased hydrophobicity could also be due to larger density of TCMS coating at the surface.

The presence of silicon on the papers was confirmed by energy dispersive X-ray spectroscopy. The EDS spectra for each type of paper are shown below the corresponding SEM images in Fig. 3. Each of the EDS spectra contains carbon and oxygen peaks both from the paper itself and the silane reagents. For the coated papers, each spectrum also has a silicon peak that is not observed on uncoated paper, providing evidence for the presence of the desired reaction product. In addition, a fluorine peak is observed for the TCFS-coated paper, providing further evidence of successful surface modification. Taking into account optimal coating time (~5 min), similarity of paper morphology to uncoated papers, and hydrophobicity of the paper (>130° by CAG), TCMS and TCOS were chosen as the initial primary coating agents for the paper substrates.

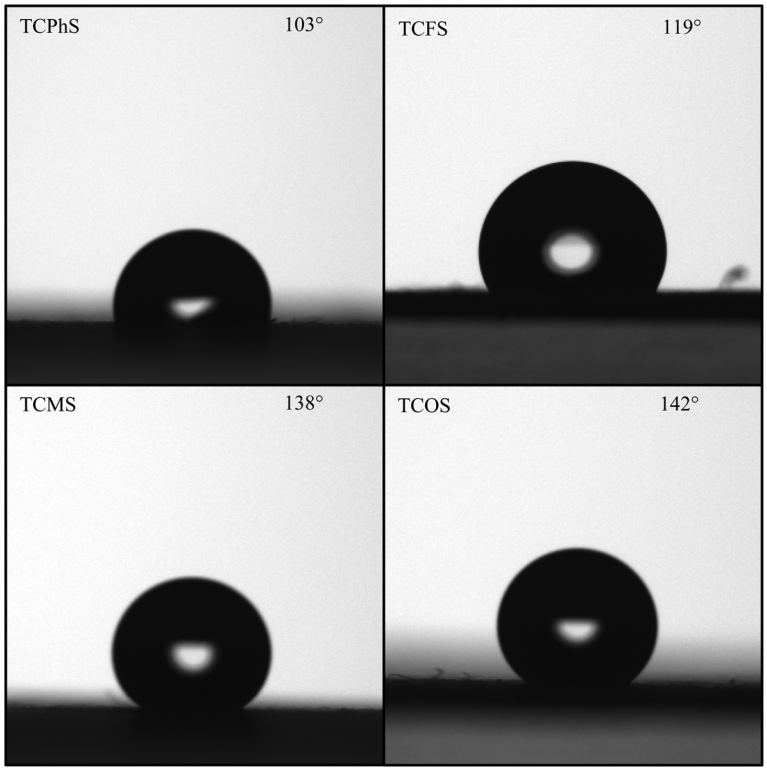

Fig. 2 Sample contact angle images and angles for paper substrates coated with TCPhS, TCFS, TCMS, and TCOS. Each of the images was collected after immersing the papers for 2 h in 50 mM of their respective silanes.

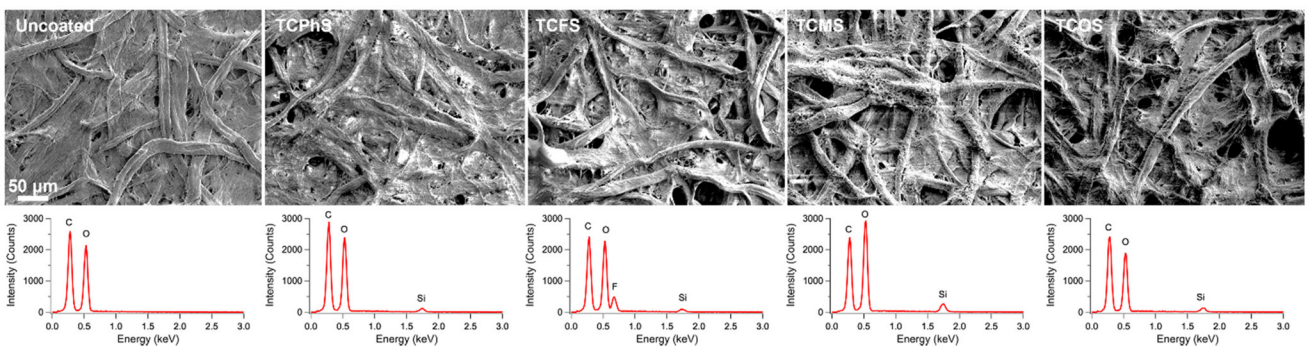

Fig. 3 SEM images for an uncoated paper substrate and paper substrates coated with 50 mM of each silane for two hours (top) with corresponding EDS spectra (bottom). All SEM images were collected at 300× magnification and a probe current of 38.0 with the secondary electron detector. The beam voltage was 1.5 kV for the uncoated paper and was 2.0 kV for all of the coated papers.

Patterning

In order to optimize the patterning parameters for different channel widths, we designed a 3D-printed mask with varying channel widths, shown in Fig. 4A. The mask is made of orange plastic (PLA), and the channels nominally ranged from 0.5 mm to 2.5 mm, in 0.5 mm increments. When measured with a set of calipers, the channel widths on the printed masks were each ~0.1 mm wider than the nominal width. Two sample papers after silane coating and oxygen/plasma treatment are shown in Fig. 4B and C with dye (food coloring in water) added to visualize the patterned area. These initial results indicated that dimensional control was better with the TCMS-treated papers. On the TCMS paper (Fig. 4B), the channels were well-defined, with the shape of the pattern closing mimicking that of the mask. On the TCOS paper (Fig. 4C), the patterned area appeared to extend well beyond the boundaries defined by the mask. Of note, the channels at the bottom of the feature were much wider than those on the mask, and the two channels on the far left began to overlap. The better-defined features on the TCMS-coated paper may be because surface methyl groups from TCMS are easier to oxidize more

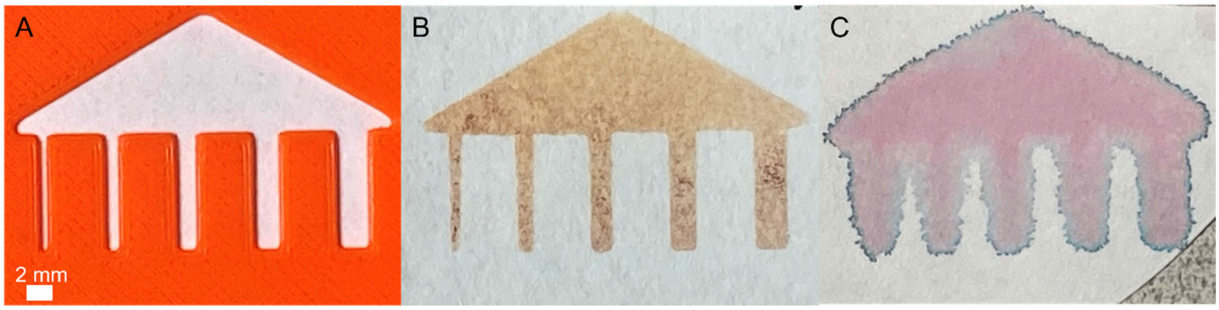

Fig. 4 (A) Sample mask made in orange plastic. (B) Paper coated with TCMS and patterned with oxygen plasma, with dye added to visualize the channels. (C) Paper coated with TCOS and patterned with oxygen plasma, with dye added to visualize the channels.

uniformly than the surface octyl groups from TCOS, or that the TCMS coating is more uniform and/or denser prior to patterning. TCMS might not only be denser on the paper surface but may also penetrate deeper into the fibrous structure of the paper. From these initial results, we chose to further optimize channel dimensions with TCMS-coated paper substrates.

After selecting TCMS as the coating agent for our filter paper substrates (50 mM in hexane for 5 min), we optimized dimensional control by exploring mask thickness, oxygen/plasma intensity, and time exposed to oxygen/plasma treatment. We made multiple masks similar to that in Fig. 4 with thicknesses varying from 1 to 3 mm. Measured channel width on the paper as a function of mask channel width is shown for the 2-mm thick mask in Fig. 5. Graphs for other mask thicknesses are provided in the ESI (Fig. S1–S4†). Food coloring in water was added to the patterned substrate, and the widths of the colored regions were measured using calipers. Each data point on the graph is an average of three measurements from three separate patterned substrates, and the error bars represent the standard deviation of these measurements. We tested three intensities (low, medium, high) and three exposure times (5, 10, 20 s). The black dashed-dotted line represents the target channel widths, and the points and error bars represent channel widths measured from 3 different paper substrates after the addition of dye. For this mask, no channels were formed under low intensity for 5 s, and only the 2.5 mm channel formed under low intensity for 10 s. Several conditions resulted in channel widths close to the targets: low (20 s), medium (5 and 10 s), and high (5 s). Under high and medium intensities for longer times, the papers were overexposed and had measured channel widths much larger than the targets. As expected, measured channel width was a function of all three variables. In general, a thicker mask and lower intensity required longer optimal exposure times. For example, the optimal intensity and exposure times for the 3-mm thick mask (Fig. S4†) were medium for 10 s and high for 5 s, and no channels were formed under low intensity (up to 20 s exposure). In contrast, the optimal intensity and exposure times for the 1 mm thick mask (Fig. S1†) were low for 10 or 20 s and medium for 5 s.

Triangular paper substrates for paper spray required slightly different patterning parameters for optimal channel widths compared to the larger substrate, but the trends from the larger substrates provided a useful starting point. A picture showing each of the masks for the paper triangles is shown in Fig. 6A. Fig. 6B shows coated and patterned paper triangles for each of the target channel widths (with dye added for visualization). Optimum conditions for each channel width are shown in Table S1.† The optimum time of exposure varied, but low intensity was used in all cases. While similar channels

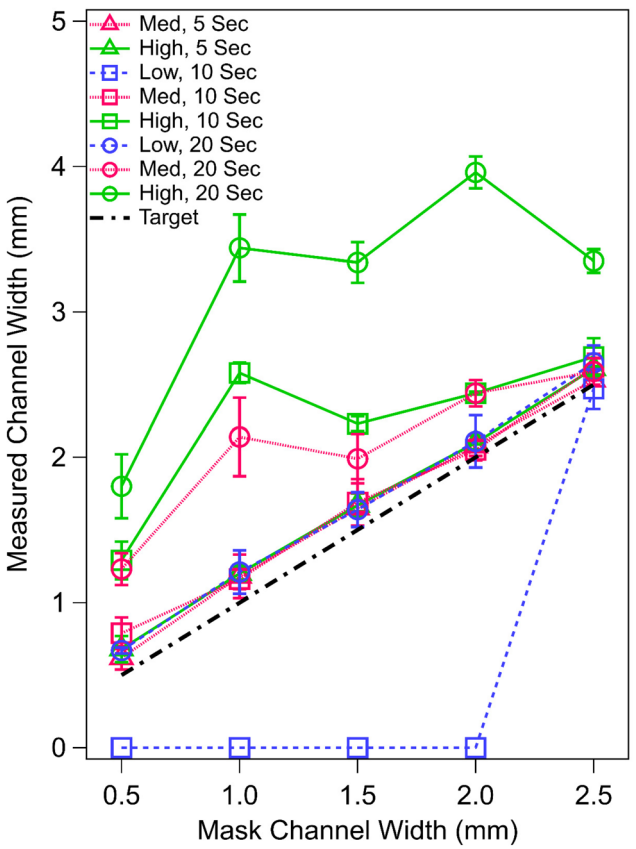

Fig. 5 Measured channel width as a function of mask channel width for a 2-mm thick mask for 8 different oxygen plasma conditions from papers coated with 50 mM TCMS for 5 min. The dashed line indicated the target channel width. No channels were formed when the plasma cleaner was set at low for 5 seconds.

could sometimes be generated between low, medium, and high intensities, dimensional control tended to be more consistent with lower intensities.

Before performing paper spray mass spectrometry, the effect of solvent composition on observed channel width on the paper was investigated. Varying mixtures of water and methanol from 95/5 (methanol/water, v/v) to 0/100 (methanol/water, v/v) were tested. Previous studies with wax and paraffin barriers on paper substrates have been used with methanol content up to 80% with wax barriers[43,45] and up to 100% with paraffin.[44] Sample papers spotted with these mixtures in 5% composition increments are shown in Fig. S5.† More polar solvent ratios were expected to be contained more within the channels, and that was the trend observed. At room temperature, the channels became undefined above about 50% methanol. Interestingly, we observed a temperature effect when testing the solvent composition. In Fig. S5A,† the channels with solvent added are shown immediately after mixing, and the exothermic mixing of water and methanol resulted in an elevated solvent temperature. In Fig. S5B,† the solvents were left to sit on the bench overnight and then added to the papers. In Fig. S5C,† the solvents were stored in the fridge overnight at 4 °C and then added to the papers. At higher solvent temperatures, the channels became less defined at lower ratios of the methanol water mixture. At lower temperatures, the channels remained more defined up to about 50% methanol. This observation may be due to lower solvent viscosity at higher temperatures, which could enable the solvent to spread more easily on the surface of the paper. We chose to use cold 50/50 methanol/water for all our experiments to ensure the best definition of the filled channels possible while maintaining maximum organic content.

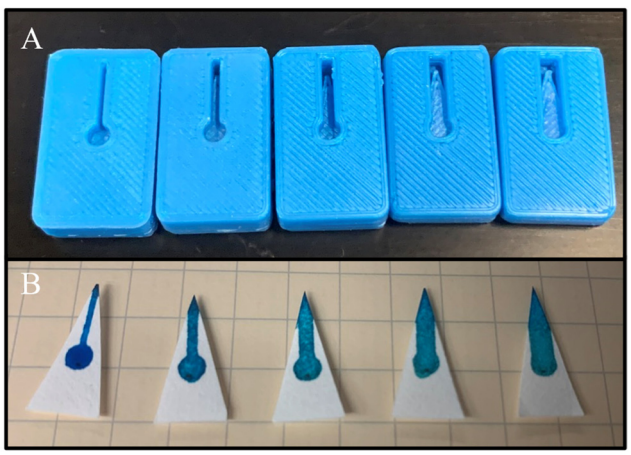

Fig. 6 (A) 3D-printed masks made from PLA for each channel width, ranging from 0.5 mm to 2.5 mm, shown in 0.5 mm increments from left to right. The outer dimensions of the masks are 15 × 25 mm. (B) Paper substrates corresponding to the masks above, coated with TCMS (50 mM in hexane, 5 min) and patterned *via* oxygen/plasma with dye added to visualize the channels. The paper dimensions are 8 × 16 mm (base × height).

Paper spray mass spectrometry

We generated calibration curves for each of the four ARVs analyzed for patterned paper substrates at each channel width as well as uncoated paper substrates. Sample calibration curves comparing substrates with 2-mm channels to uncoated substrates are shown in Fig. 7. Sample MS/MS spectra for each analyte are shown in Fig. 8. Calibration curves for the other channel widths tested can be found in the ESI (Fig. S6–S9†). The *x*-axis for each calibration plot shows the concentration in ng mL^{-1} and the *y*-axis shows the ratio of the area of the analyte peak (A) to the area of the internal standard peak (IS). Error bars represent the standard error of three replicate paper substrates. For each of the analytes and channel widths tested, the sensitivity (slope of the curve) was greater for all patterned papers versus the uncoated papers. The increases in slope over uncoated substrates ranged from 2.5-fold up to 19-fold, with an average increase of 7.2-fold across all channel widths and drugs tested. Every channel width showed an improvement in sensitivity for every drug, but it is worth noting that the improvement varied depending on drug and channel width. Similar variation was observed in the limits of detection and quantification.

The limits of detection (LODs) and limits of quantification (LOQs) for each drug and type of paper substrate are shown in Table 1. LODs were calculated as $3\sigma_{blank}/m$ and LOQs as $10\sigma_{blank}/m$, where σ_{blank} was the standard deviation of the blank and m was the slope of the calibration curve. Every channel width for the patterned papers showed improved LODs and LOQs over the uncoated paper substrates. In the case of FTC analyzed with the uncoated papers, the highest calibration level (1250 ng mL^{-1}) was below the LOQ (2200 ng mL^{-1}) and was the only calibration level above the LOD (670 ng mL^{-1}). For comparison, the highest LOQ was 200 ng mL^{-1} for the patterned papers, and the lowest was 24 ng mL^{-1}. The increase in sensitivity and improvements in LOD/LOQ are likely due to multiple factors. First, the patterned papers required lower volumes of solvent to sustain a stable electrospray for the time required to collect the mass spectra (<10 μL for patterned *vs.* 20 μL for uncoated). This results in a smaller dilution factor – and therefore higher concentration – for the analytes after extraction for the patterned paper substrates. Second, the pattern of the substrates directs all the solvent and sample toward the mass spectrometer, likely resulting in more efficient delivery of analytes compared to uncoated papers. In the case of the uncoated papers, both analyte and solvent spread throughout the entirety of the surface of the substrate. Finally, there may be changes in spray dynamics, fluid flow rate, or ionization efficiency that improve detection. These will be the subject of future work.

In general, the detection limits from lowest to highest at a given channel width were: DTG, 3TC, EFV, and FTC. The difference in detection limits is probably due to a combination of physicochemical properties of the antiretrovirals studied and their interactions with the paper substrates and solvent. For example, 3TC is the most polar of the drugs studied ($\log P$ = −1.4), and EFV is the most nonpolar ($\log P$ = 4.6). DTG ($\log P$ =

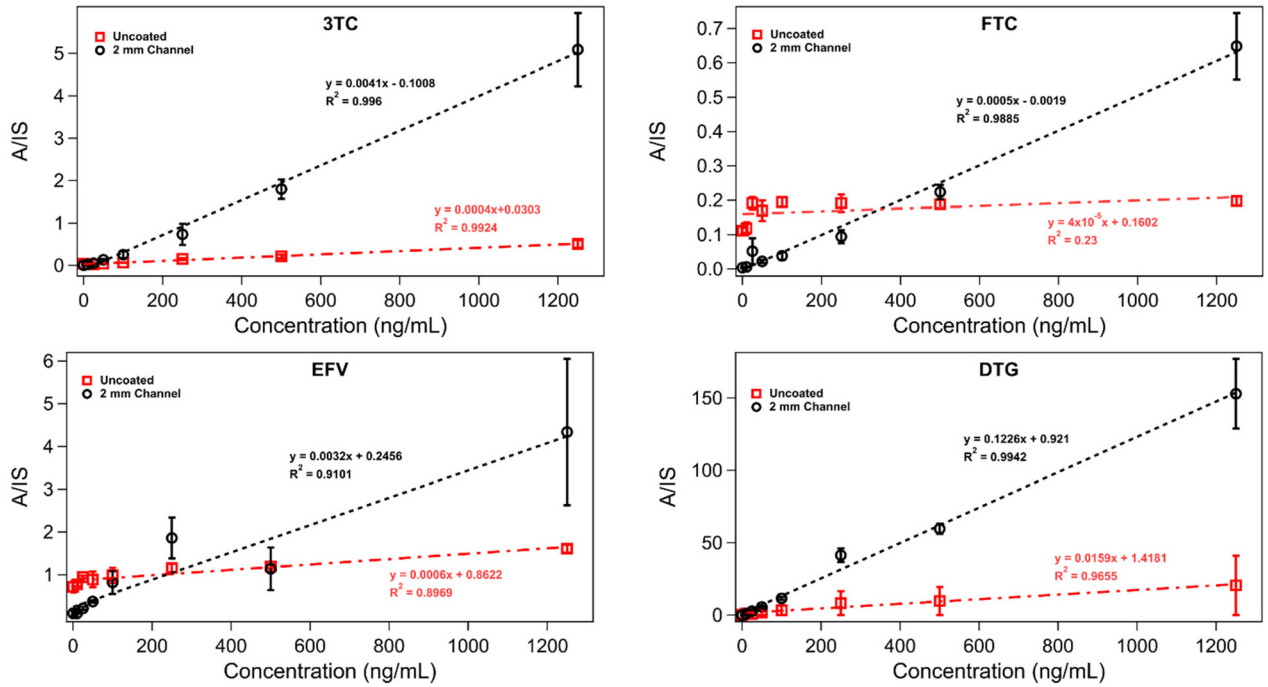

Fig. 7 Calibration curves for uncoated (red squares) and patterned papers with 2-mm channels (black circles) for four target antiretrovirals in methanol/water. The *y*-axis is the area of the analyte peak (A) divided by the area of the internal standard peak (IS). The error bars represent the standard error of 3 measurements.

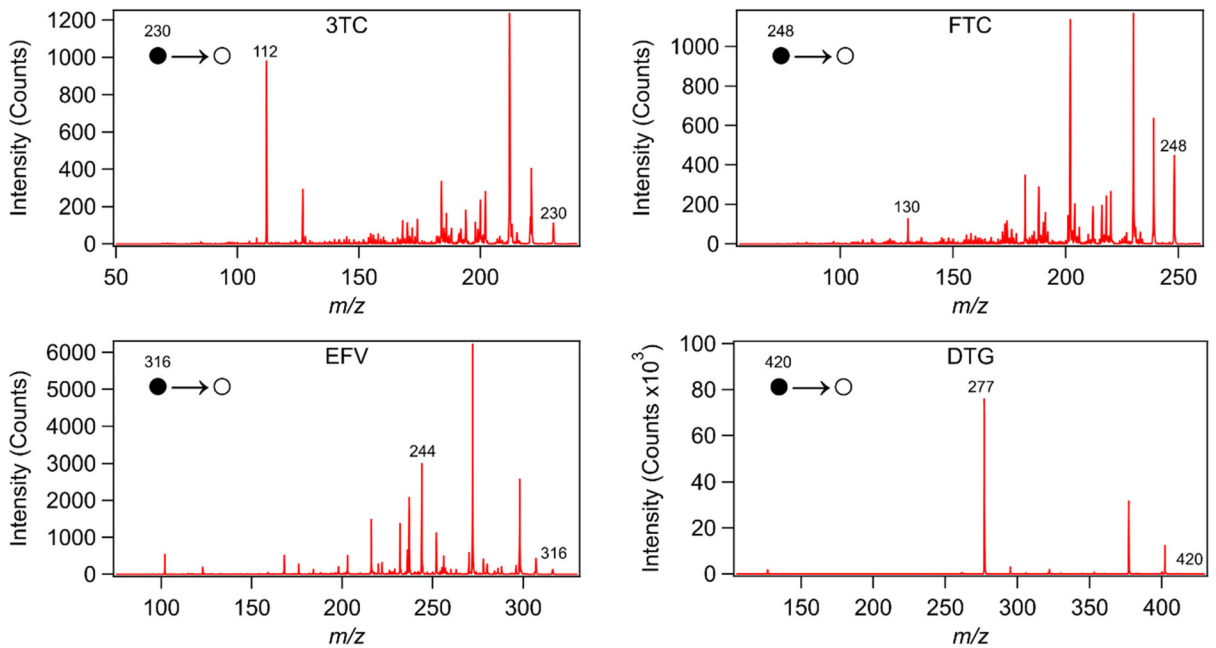

Fig. 8 Sample MS/MS spectra for each of the four antiretrovirals analyzed in the study. The spectrum for each drug is labeled accordingly: lamivudine (3TC), emtricitabine (FTC), efavirenz (EFV), and dolutegravir (DTG). Precursor and product ions for each drug are labeled in the figure.

2.2) and FTC ($\log P = -0.4$) have polarities between those two. Thus, the observed trend in detection limits cannot be explained by polarity alone. Similarly, the trend cannot be explained only by mass (DTG > EFV > FTC > 3TC) or basicity (EFV > DTG > FTC > 3TC). We plan to continue investigating these trends.

Interestingly, within a drug type, there was no clear trend in channel width versus LOD/LOQ for any of the drugs tested

Table 1 Limits of detection and quantification for each drug and channel width examined in methanol/water

	Drug type							
	3TC		FTC		EFV		DTG	
Channel widths (mm)	LOD	LOQ	LOD	LOQ	LOD	LOQ	LOD	LOQ
Uncoated	160	550	670	2200	620	2100	9.8	33
0.5	0.77	2.6	14	48	1.8	6.0	0.10	0.34
1	1.8	6.1	59	200	4.1	14	0.014	0.048
1.5	1.9	6.5	60	200	3.1	10	0.019	0.062
2	1.8	5.8	7.2	24	42	140	0.076	0.25
2.5	0.28	0.92	11	36	2.1	7.1	0.17	0.58

LOD: limit of detection, calculated as $3\sigma_{blank}/m$; LOQ: limit of quantification, calculated as $10\sigma_{blank}/m$. All LODs and LOQs are reported in units of ng mL^{-1}.

here. The analysis of EFV with the 2 mm channel width substrates showed higher LOD/LOQ than the other patterned papers, and the lowest LOD/LOQ for EFV was observed with the 0.5 mm channel patterned papers. This observation was not consistent across all analytes. The lowest LODs for 3TC and FTC were observed with the 2.5 mm patterned papers, and the lowest LOD for DTG was observed with the 1 mm patterned papers. LODs and LOQs, as well as overall precision, would likely be improved with the use of isotopically labeled internal standards.

Detection of ARVs in urine samples

After seeing the initial improvement of the patterning approach, we tested the performance of our patterned substrates by spiking ARVs into human urine. We generated calibration curves for each of the four ARVs using the 2-mm channel width paper substrates and compared the results to uncoated paper substrates. The curves for each drug and substrate are shown in Fig. 9. The *x*-axis for each calibration curve shows the concentration in ng mL^{-1} and the *y*-axis shows the ratio of the area of the analyte peak (A) to the area of the internal standard peak (IS). Error bars represent the standard error of three replicate paper substrates. Similar to the methanol/water matrix, a general improvement in sensitivity and LODs/LOQs was seen for the patterned substrates over the uncoated substrates. The average improvement in sensitivity for the patterned paper substrates was 7.4-fold, which was similar to that observed for the patterned papers over the

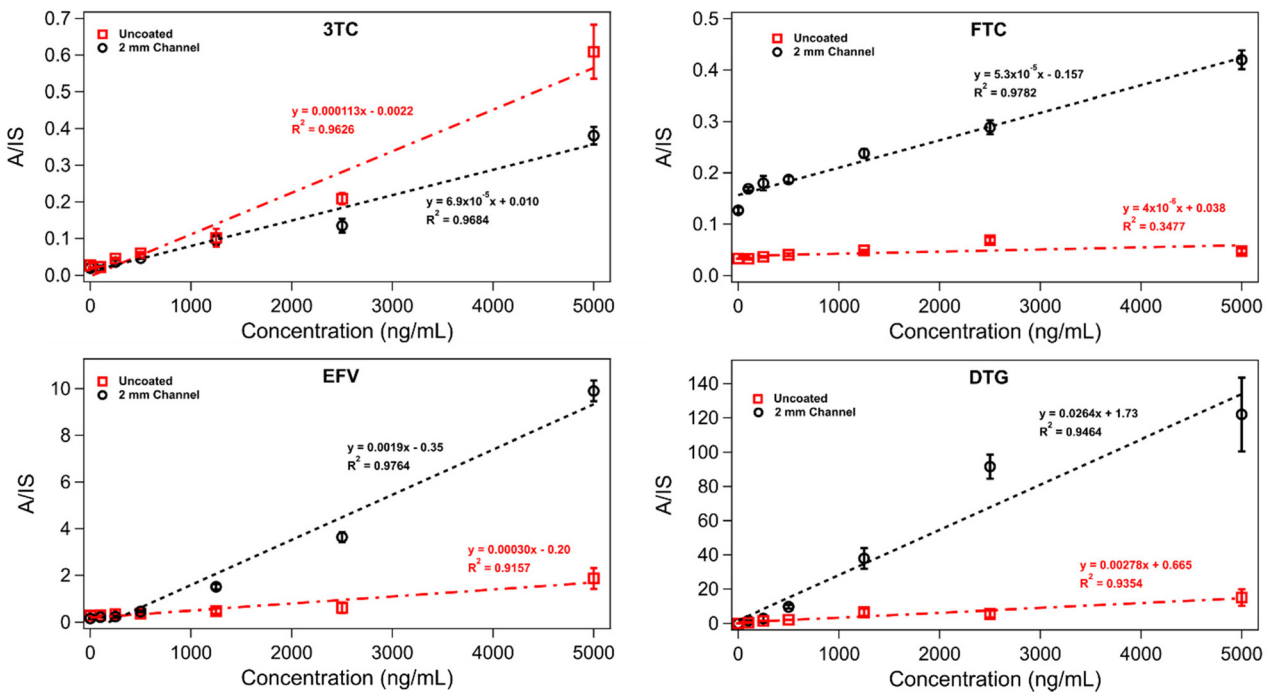

Fig. 9 Calibration curves for uncoated (red squares) and patterned papers with 2 mm channels (black circles) for four target antiretrovirals spiked in urine. The *y*-axis is the area of the analyte peak (A) divided by the area of the internal standard peak (IS). The error bars represent the standard error of 3 measurements.

Table 2 Limits of detection and quantification for each drug and channel width examined in urine

	Drug type							
	3TC		FTC		EFV		DTG	
Channel widths (mm)	LOD	LOQ	LOD	LOQ	LOD	LOQ	LOD	LOQ
Uncoated	165	551	424	1410	129	430	9.9	33
2	86.8	289	307	1020	4.3	14	0.25	0.84

LOD: limit of detection, calculated as $3\sigma_{blank}/m$; LOQ: limit of quantification, calculated as $10\sigma_{blank}/m$. All LODs and LOQs are reported in units of ng mL^{-1}.

uncoated papers in the methanol/water matrix (7.2-fold). For FTC, EFV, and DTG, the improvement in sensitivity ranged from 13-fold for FTC to 95-fold for DTG. For 3TC, the patterned papers and uncoated papers showed similar sensitivities, with the sensitivity of the patterned paper substrates approximately 60% of the sensitivity of the uncoated substrate. The LODs and LOQs each of the ARVs in the urine samples are shown in Table 2. The patterned paper substrates showed an improvement in LOD and LOQ for each of the four drugs, with an average improvement of about 18-fold.

There was a predictable decrease in sensitivity and increase in LODs/LOQs when switching from a neat matrix (methanol/water) to a biological matrix (urine) for the patterned papers. For the uncoated paper substrates, many of the LODs were lower for urine than they were for the neat matrix, despite lower sensitivity for all drugs. This change is due to lower standard deviation of the blank samples, pointing to data collection with better reproducibility than that of the methanol/water samples, which may be a result of more consistent non-zero background from the more complex urine matrix. The changes in sensitivity and LODs for the patterned papers are expected and likely due to ion suppression from the presence of salts and other interfering compounds, commonly seen with paper spray mass spectrometry.[6,11] Other groups have attempted to overcome this limitation by changing solvents or performing a limited amount of sample preparation (*i.e.* extraction).[11,53–55] These and other strategies will be a focus for improving sensitivity and LODs for our methods in the future.

Conclusion

In this study, we present a method for coating and patterning paper substrates for PS-MS. Papers were modified using silane reagents to produce a hydrophobic coating before patterning a hydrophilic channel *via* 3D-printed masks and surface oxidation with oxygen/plasma exposure. TCMS and TCOS were initially chosen as primary coating agents as they produced optimal coating parameters. Coating time, surface morphology, and hydrophobicity of the papers were characterized using SEM, EDS, and CAG. TCMS was found to provide better dimensional control over the patterned papers as demonstrated through the more defined filled channels on TCMS-treated papers than TCOS-treated papers. Optimal intensity and exposure times were developed for paper spray substrates with channels ranging from 0.5 to 2.5 mm in width. Solvent composition was also studied, and we found that cold 50/50 methanol/water produced the most defined channel while maintaining maximum organic content. PS-MS was performed to detect four different ARVs for all five channel widths. Improved sensitivity, LOD, and LOQ were observed for each of the patterned substrates compared to the uncoated substrates. Spiked urine samples were analyzed by PS-MS with uncoated and a 2 mm patterned substrate. The patterned substrates showed improved in sensitivity for three of the four target drugs and improved LOD and LOQ for all of the target drugs. Future work will include exploration of other channel geometries as well as sample preparation and analysis strategies for improved detection in biological matrices.

Author contributions

Austin Arias coated paper substrates, explored optimum solvent composition, optimized patterning for one of the channel widths studied, and produced calibration curve and MS/MS figures. Peyton Windham optimized patterning parameters for most of the channel widths, produced most of the substrates for calibration experiments, performed the initial experiments with ARVs in urine, and created the LOD/LOQ tables and figure with paper triangles and masks. Natalie Cheyne performed coating experiments and measured contact angles. Mac Gilliland collected most of the SEM and EDS data in the article and performed the calibration curve experiments in the lab.

Conflicts of interest

The authors declare no potential conflicts of interest.

Acknowledgements

Research reported in this publication was supported by the National Institute of General Medical Sciences of the National Institutes of Health under Award Number P20GM103499. The

content is solely the responsibility of the authors and does not necessarily represent the official views of the National Institutes of Health. This material is based upon work supported by the National Science Foundation under Grant No. CHE-1757706. The authors also gratefully acknowledge the Furman University Office of Undergraduate Research and Furman University start-up funds.

References

1 C. L. Feider, A. Krieger, R. J. Dehoog and L. S. Eberlin, *Anal. Chem.*, 2019, **91**, 4266–4290.
2 T. H. Kuo, E. P. Dutkiewicz, J. Pei and C. C. Hsu, *Anal. Chem.*, 2020, **92**, 2353–2363.
3 Z. Takáts, J. M. Wiseman, B. Gologan and R. G. Cooks, *Science*, 2004, **306**, 471–473.
4 R. G. Cooks, Z. Ouyang, Z. Takats and J. M. Wiseman, *Science*, 2006, **311**, 1566–1570.
5 R. B. Cody, J. A. Laramée and H. D. Durst, *Anal. Chem.*, 2005, **77**, 2297–2302.
6 H. Wang, J. Liu, R. Graham Cooks and Z. Ouyang, *Angew. Chem., Int. Ed.*, 2010, **49**, 877–880.
7 C. B. Nguyen, W. R. A. Wichert, D. O. Carmany, E. M. McBride, P. M. Mach, E. S. Dhummakupt, T. Glaros and N. E. Manicke, *Anal. Chem.*, 2021, **93**, 13467–13474.
8 E. S. Dhummakupt, D. O. Carmany, P. M. Mach, T. M. Tovar, A. M. Ploskonka, P. S. Demond, J. B. DeCoste and T. Glaros, *ACS Appl. Mater. Interfaces*, 2018, **10**, 8359–8365.
9 A. E. O'Leary, S. E. Hall, K. E. Vircks and C. C. Mulligan, *Anal. Methods*, 2015, **7**, 7156–7163.
10 P. W. Fedick, B. J. Bills, N. E. Manicke and R. G. Cooks, *Anal. Chem.*, 2017, **89**, 10973–10979.
11 E. L. Rossini, D. S. Kulyk, E. Ansu-Gyeabourh, T. Sahraeian, H. R. Pezza and A. K. Badu-Tawiah, *J. Am. Soc. Mass Spectrom.*, 2020, **31**, 1212–1222.
12 C. J. Pulliam, R. M. Bain, J. S. Wiley, Z. Ouyang and R. G. Cooks, *J. Am. Soc. Mass Spectrom.*, 2015, **26**, 224–230.
13 S. L. Reeber, S. Gadi, S. B. Huang and G. L. Glish, *Anal. Methods*, 2015, **7**, 9808–9816.
14 S. Maher, F. P. M. Jjunju, D. E. Damon, H. Gorton, Y. S. Maher, S. U. Syed, R. M. A. Heeren, I. S. Young, S. Taylor and A. K. Badu-Tawiah, *Sci. Rep.*, 2016, **6**, 1–10.
15 F. P. M. Jjunju, S. Maher, D. E. Damon, R. M. Barrett, S. U. Syed, R. M. A. Heeren, S. Taylor and A. K. Badu-Tawiah, *Anal. Chem.*, 2016, **88**, 1391–1400.
16 I. Mahmud, F. G. Pinto, V. Y. Rubio, B. Lee, C. P. Pavlovich, R. J. Perera and T. J. Garrett, *Anal. Chem.*, 2021, **93**, 7774–7780.
17 J. A. Michely, M. R. Meyer and H. H. Maurer, *Anal. Chem.*, 2017, **89**, 11779–11786.
18 C. Zhang and N. E. Manicke, *Anal. Chem.*, 2015, **87**, 6212–6219.
19 R. Jett, C. Skaggs and N. E. Manicke, *Anal. Methods*, 2017, **9**, 5037–5043.
20 S. Chiang, W. Zhang and Z. Ouyang, *Expert Rev. Proteomics*, 2018, **15**, 789.
21 S. Chen, Q. Wan and A. K. Badu-Tawiah, *J. Am. Chem. Soc.*, 2016, **138**, 6356–6359.
22 N. E. Manicke, Q. Yang, H. Wang, S. Oradu, Z. Ouyang and R. G. Cooks, *Int. J. Mass Spectrom.*, 2011, **300**, 123–129.
23 J. V. Coelho Pimenta, R. Augusti and A. A. Sabino, *J. Am. Soc. Mass Spectrom.*, 2021, **32**, 2168–2174.
24 X. Zhou, J. Pei and G. Huang, *Rapid Commun. Mass Spectrom.*, 2015, **29**, 100–106.
25 D. Sarkar, A. Som and T. Pradeep, *Anal. Chem.*, 2017, **89**, 11378–11382.
26 S. Banerjee, C. Basheer and R. N. Zare, *Angew. Chem., Int. Ed.*, 2016, **55**, 12807–12811.
27 R. M. Bain, C. J. Pulliam, S. A. Raab and R. G. Cooks, *J. Chem. Educ.*, 2016, **93**, 340–344.
28 J. Li, Y. Zheng, W. Mi, T. Muyizere and Z. Zhang, *Anal. Methods*, 2018, **10**, 2803–2811.
29 T. Wang, Y. Zheng, X. Wang, D. E. Austin and Z. Zhang, *Anal. Chem.*, 2017, **89**, 7988–7995.
30 Y. Zheng, Q. Wang, X. Wang, Y. Chen, X. Wang, X. Zhang, Z. Bai, X. Han and Z. Zhang, *Anal. Chem.*, 2016, **88**, 7005–7013.
31 Y. Zheng, X. Zhang, H. Yang, X. Liu, X. Zhang, Q. Wang and Z. Zhang, *Anal. Methods*, 2015, **7**, 5381–5386.
32 Q. Wang, Y. Zheng, X. Zhang, X. Han, T. Wang and Z. Zhang, *Analyst*, 2015, **140**, 8048–8056.
33 P. W. Fedick, F. Pu, N. M. Morato and R. G. Cooks, *J. Am. Soc. Mass Spectrom.*, 2020, **31**, 735–741.
34 D. S. Burr, W. L. Fatigante, J. A. Lartey, W. Jang, A. R. Stelmack, N. W. McClurg, J. M. Standard, J. R. Wieland, J. H. Kim, C. C. Mulligan and J. D. Driskell, *Anal. Chem.*, 2020, **92**, 6676–6683.
35 X. Wang, Y. Zheng, T. Wang, X. Xiong, X. Fang and Z. Zhang, *Anal. Methods*, 2016, **8**, 8004–8014.
36 E. S. Dhummakupt, D. O. Carmany, P. M. Mach, T. M. Tovar, A. M. Ploskonka, P. S. Demond, J. B. DeCoste and T. Glaros, *ACS Appl. Mater. Interfaces*, 2018, **10**, 8359–8365.
37 P. Basuri, A. Baidya and T. Pradeep, *Anal. Chem.*, 2019, **91**, 7118–7124.
38 D. E. Damon, K. M. Davis, C. R. Moreira, P. Capone, R. Cruttenden and A. K. Badu-Tawiah, *Anal. Chem.*, 2016, **88**, 1878–1884.
39 D. E. Damon, M. Yin, D. M. Allen, Y. S. Maher, C. J. Tanny, S. Oyola-Reynoso, B. L. Smith, S. Maher, M. M. Thuo and A. K. Badu-Tawiah, *Anal. Chem.*, 2018, **90**, 9353–9358.
40 Z. Chen, Q. Shi, W. Wang, Z. Jiang, G. L. Zhang, L. Tong, X. Mu and B. Tang, *Anal. Chem.*, 2021, **93**, 1749–1756.
41 J. Liu, Y. He, S. Chen, M. Ma, S. Yao and B. Chen, *Talanta*, 2017, **166**, 306–314.
42 T. Zargar, T. Khayamian and M. T. Jafari, *Microchim. Acta*, 2018, **185**, 1–9.
43 I. Murray, G. Walker and M. S. Bereman, *Analyst*, 2016, **141**, 4065–4073.

44 T. C. Colletes, P. T. Garcia, R. B. Campanha, P. V. Abdelnur, W. Romão, W. K. T. Coltro and B. G. Vaz, *Analyst*, 2016, **141**, 1707–1713.
45 D. E. Damon, Y. S. Maher, M. Yin, F. P. M. Jjunju, I. S. Young, S. Taylor, S. Maher and A. K. Badu-Tawiah, *Analyst*, 2016, **141**, 3866–3873.
46 S. Azizov, M. Sharipov, J. M. Lim, S. M. Tawfik, N. Kattaev and Y. I. Lee, *J. Mass Spectrom.*, 2021, **56**, e4611.
47 S. Jackson, S. Lee and A. K. Badu-Tawiah, *Anal. Chem.*, 2022, **94**, 5132–5139.
48 Q. He, C. Ma, X. Hu and H. Chen, *Anal. Chem.*, 2013, **85**, 1327–1331.
49 M. Hashemi Hedeshi, O. Rezvani and H. Bagheri, *Anal. Chim. Acta*, 2020, **1128**, 31–41.
50 Y. Zhang, T. Ren and J. He, *ACS Appl. Mater. Interfaces*, 2018, **10**, 11343–11349.
51 FDA Drug Data, **https://www.accessdata.fda.gov/**, accessed 30 August 2023.
52 P. Samyn, *J. Mater. Sci.*, 2013, **48**, 6455–6498.
53 S. A. Borden, A. Saatchi, J. Palaty and C. G. Gill, *Analyst*, 2022, **147**, 3109–3117.
54 F. M. de Oliveira, G. L. Scheel, R. Augusti, C. R. T. Tarley and C. C. Nascentes, *Anal. Chim. Acta*, 2020, **1106**, 52–60.
55 Y. Yang, J. Wu, J. Deng, K. Yuan, X. Chen, N. Liu, X. Wang and T. Luan, *Anal. Chim. Acta*, 2018, **1032**, 75–82.